Available online at www.sciencedirect.com

SCIENCE DIRECT

Intermetallics 12 (2004) 1097–1102

Intermetallics

www.elsevier.com/locate/intermet

# Deformation morphology underneath the Vickers indent in a Zr-based bulk metallic glass

S. Jana[a], R. Bhowmick[a], Y. Kawamura[b], K. Chattopadhyay[a], U. Ramamurty[a,*]

[a]Department of Metallurgy, Indian Institute of Science, C.V. Raman Avenue, Bangalore 560 012, India

[b]Department of Mechanical Engineering and Materials Science, Kumamoto University, 2-39-1 Kurokami, Kumamoto 860-8555, Japan

Available online 20 May 2004

**Abstract**

Hardness and plastic deformation during Vickers indentation in as-cast, annealed, and fully crystallized $Zr_{57}Cu_{27}Al_{11}Ni_5$ bulk metallic glass was examined. Subsurface deformation morphology under the indenter tip was studied at various loads and for different annealing time. Appreciable plastic deformation, through shear banding, occurs in the as-cast and annealed alloys. Two different types of shear bands are observed. Their occurrence depends upon the amount of annealing and hence on the extent of crystallization. The fully crystallized alloy exhibits extensive cracking. Trends in the deformation zone size with load are consistent with the expanding cavity model, while the shear band morphology, particularly for the as-cast sample, attests the qualitative applicability of the slip line field theory.



*Keywords:* B. Glasses, metallic; B. Mechanical properties at ambient temperature; B. Plastic deformation mechanisms; C. Heat treatment; F. Mechanical testing

## 1. Introduction

Understanding the micro-mechanisms of plastic deformation and developing the constitutive relationships for bulk metallic glasses (BMGs) is an active area of research. Indentation test is an excellent means for such studies, especially since it needs only a small volume of material [1–10]. This study examines the Vickers hardness and the associated deformation morphology in a Zr-based BMG. Particular emphasis was on elucidating the subsurface deformation morphology, obtained through the bonded interface technique. Recent research has shown that hardness and strength of BMGs can be improved by inducing partial crystallization [12–14]. However, the impact toughness of the annealed BMGs drops precipitously [15]. It is not clear whether the loss in toughness is primarily due to the loss in the deformability of the BMGs upon partial crystallization. This study, by examining the indentation response of annealed alloys, aims at developing some basic mechanistic understanding of the associated changes in the deformation behavior of BMGs.

* Corresponding author. Tel.: +91-80-2293-3241; fax: +91-80-2360-0472.

*E-mail address:* ramu@met.iisc.ernet.in (U. Ramamurty).

0966-9795/$ - see front matter © 2004 Elsevier Ltd. All rights reserved.
doi:10.1016/j.intermet.2004.04.018

## 2. Materials and experiments

Two millimeters thick plates of the $Zr_{57}Cu_{27}Al_{11}Ni_5$ BMG were processed by melting pure metals in an argon atmosphere and then chill-casting in a copper mould. The as-cast alloy was characterized using X-ray diffraction, differential scanning calorimetry (DSC), and transmission electron microscopy (TEM). To introduce partial crystallinity, the as-cast BMG was annealed at 440 °C for 30 min whereas annealing for 2 h resulted in a fully crystalline alloy. Specimens were first cut into two halves, the cut surfaces polished to a 1 μm finish and then bonded back using a high strength adhesive. Bonded specimens were put into PVC moulds and filled with cold mount resin to minimize the bond layer thickness and obtain a high strength bond. The top surface was polished so that the indentation face is flat. Vickers indentation tests were performed on the bonded interface as well as away from it. For the former, it was ensured that one of the indentation diagonal coincides with the interface. The bond was opened subsequently by dissolving the adhesive in acetone. Deformation zones, both under the indenter tip (subsurface) as well as around the bulk indentations, were examined using a scanning electron microscope.

## 3. Results

Fig. 1 shows the XRD patterns obtained from the as-cast and heat treated samples. For the as-cast alloy, broad and diffuse peak within the angular range of 30–45° followed by another weaker second broad peak within the angular range of 60–70° is seen, features characteristic of an amorphous alloy. DSC scans reveal that the glass transition temperature, $T_g$, for this alloy is ~409 °C with a single crystallization event at 472 °C, implying a super cooled liquid regime of 63 °C. The XRD pattern of the 30 min annealed alloy at 440 °C is similar to that of the as-cast alloy, implying that the crystallites are very fine sized. The XRD pattern of the fully crystallized sample shows distinct peaks, which were identified as belonging to the phases $NiZr_2$ and $AlCu_2Zr$.

Optical metallography revealed that the as-cast alloy contains occasional dendrites [16]. Electron diffraction studies in the TEM confirmed that these are $NiZr_2$ precipitates [16]. However, the absence of any crystalline peak in the XRD pattern of the as-cast alloy implies that the volume fraction of these dendrites is very small. Fig. 2 is a dark field TEM image (obtained using the second halo of the selected area diffraction (SAD) pattern shown in the inset) of the as-cast alloy showing nanometer-sized short-range order domains. The SAD pattern also shows a strong halo followed by a weak halo, which is indicative of amorphous matrix. From these observations, it appears that the as-cast alloy is a mixture of micron-sized crystallites as well as very fine nanometer-sized ordered domains embedded in a predominantly amorphous matrix.

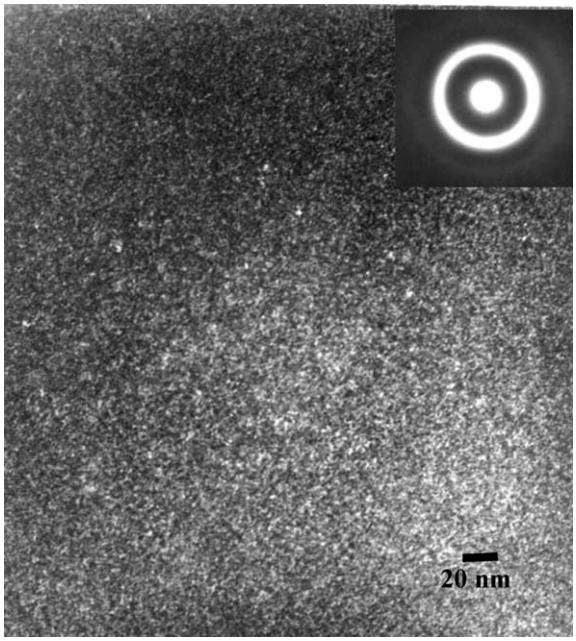


Fig. 2. Dark field TEM image of the as-cast alloy.

Fig. 3 shows the variation of the hardness, $H$, with the indentation load, $P$, for the as-cast and annealed alloys. Reliable estimates of the hardness of the fully crystallized alloy could not be obtained because of its tendency to crack. For both the as-cast and annealed alloys, a marginally higher (~5%) hardness is measured for $P$ between 50 and 2000 g, possibly a result of the indenter-tip not being sharp. Otherwise, $H$ is independent of $P$, consistent with previously reported data [11].

The average $H$ values are ~5.85 and 6.05 GPa for the as-cast and the annealed alloys, respectively. The higher

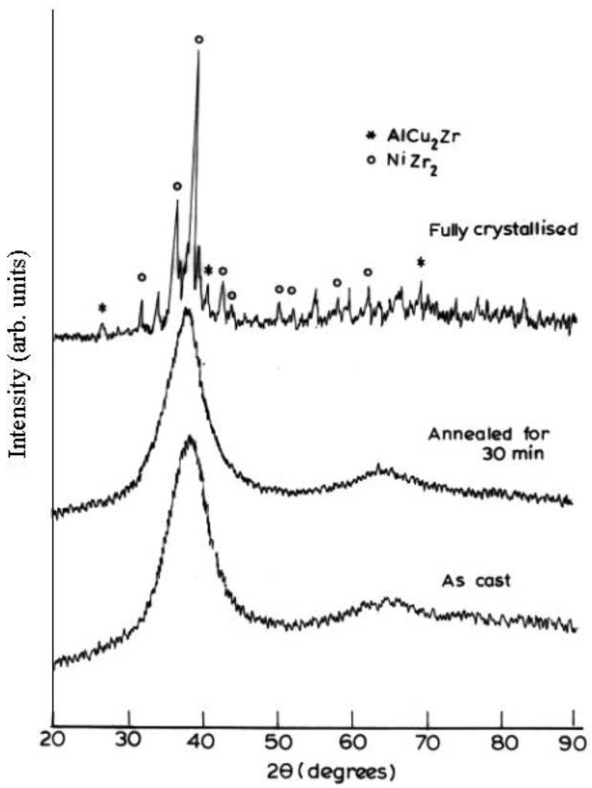


Fig. 1. XRD patterns of the as-cast and heat treated $Zr_{57}Cu_{27}Al_{11}Ni_5$ BMG.

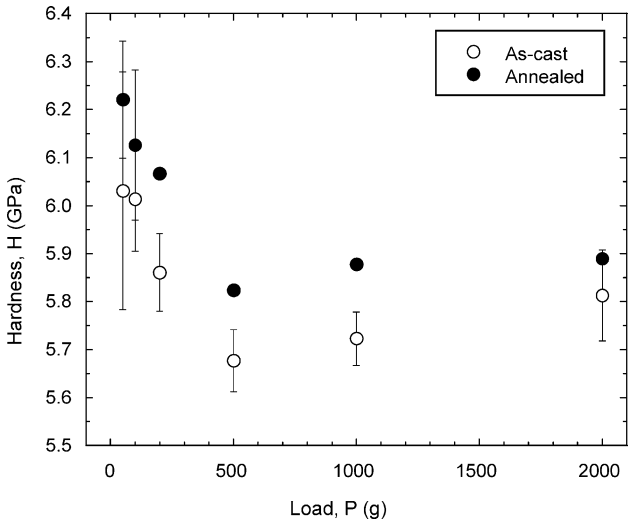


Fig. 3. Variation of the hardness with load for the as-cast and annealed alloys.

hardness of the latter is consistent with the increase in hardness with annealing that has been reported for various BMGs [14]. The plastic constraint factor, $H/Y$ (where $Y$ is the yield strength in compression) for the as-cast alloy ($Y = 1836$ MPa) is $\sim 3.2$, consistent with data reported for BMGs [9,17,18], and indicates to pressure sensitivity.

Examination of the indenter impressions shows characteristic piling up, in the form of semi-circular shear bands. Fig. 4 shows the variation of the pile-up length (i.e. distance from the center of impression to the outermost shear band), $\delta$, at different loads for the as-cast alloy. This trend can be described by using the equation $\delta = CP^{0.5}$, which is predicted using the expanding cavity model [19,20]. This model relates $C$ and $Y$ through $C = 0.691/Y^{0.5}$. However, a very large value for $Y$ ($\sim 5$ GPa) obtains with the $C$ ($\sim 0.97$ μm/g$^{1/2}$) extracted from the $\delta$ vs. $P$ curve. When $\delta$ is normalized with the diagonal length of the indentation, $D$, and plotted against $P$ (Fig. 4), it is observed that $\delta/D \sim 0.52$, except for the loads below 500 g. This trend in $\delta/D$ vs. $P$ is consistent with the trends in $H$ vs. $P$, implying slightly higher resistance for deformation at very low loads in the BMGs. The expanding cavity model predicts a constant $\delta/D$, which can be related to $Y$ through the elastic modulus and Poisson's ratio [20]. However, the predicted $Y$ is again much higher than the actual value.

Figs. 5a and 5b show the morphology of subsurface deformation in the as-cast alloys. In both the cases, a large hemispherical deformation zone is observed. The deformation morphology in the as-cast alloy, as seen in Fig. 5a is dominated by the radial shear bands and their morphology is very similar to the plastic flow field in a rigid, perfectly plastic solid subjected to plane-strain indentation. This observation suggests the applicability of the slip line field theory for explaining the plastic deformation in metallic glasses, although the assumptions inherent in that theory do not conform to the experimental conditions. For instance, the bonded interface, being highly compliant, resembles a plane stress rather than a plane strain condition that is assumed in the theory. Also the theory neglects the pressure-dependence of the yield criterion and the elasticity of the material. Another indentation, performed on the alloy with a 2000 g load, shows the semi-circular shear bands which are surface steps created due to the outward plastic flow of material into the compliant adhesive layer (Fig. 5b). Note that, in general, the subsurface morphology contains both radial and semi-circular shear bands. Depending on the relative constraint experienced by the material for its plastic flow into the bonded interface, one type of morphology dominates over the other in appearance. More the constraint at the interface, more pronounced will be the radial shear bands.

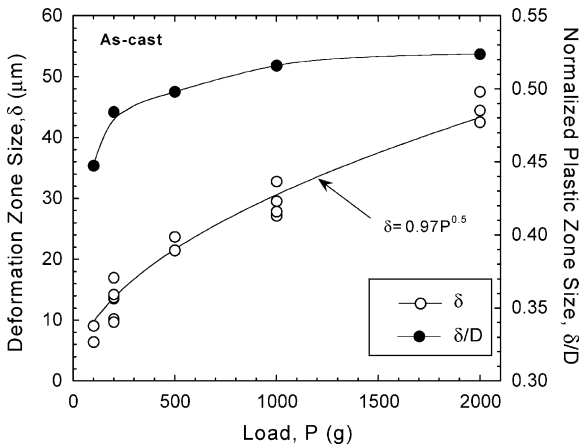


Fig. 4. Variation of the surface plastic zone length, $\delta$, plotted as a function of the indentation load for the as-cast alloy. The ratio of $\delta$ with $D$, the indenter impression diagonal is also shown.

In Fig. 5c, which shows the deformation zone for the annealed alloy, semi-circular shear bands are seen in a zone that starts from about 20 μm away from the indenter tip and extends to $\sim 80$ μm. Incipient cracking, indicated by arrows, is seen. Fig. 5d shows extensive cracking and a limited amount of shear banding outside the cracked region in the subsurface zone of the fully crystallized alloy.

Fig. 6a shows the variation of the size of subsurface deformation zone (measured from the tip of the impression to the outermost semi-circular shear band), $\lambda$, as a function of $P$, for the as-cast and annealed alloys. The trend in $\lambda$ vs. $P$ is similar to that seen in $\delta$ vs. $P$ curve in Fig. 4. Best fits to the data with $\lambda = CP^{0.5}$ yield values of 0.95 and 1.05 for $C$, for the as-cast and annealed alloys, respectively. The former is similar to the value of 0.97 obtained in the bulk indentation. Interestingly, $\lambda$ measured for the annealed alloy is marginally higher than that measured for the as-cast alloy. However, in both the cases the deformation zone size is $\sim 80$ μm at 5000 g load, indicating that both the alloys are capable of sustaining significant plastic deformation.

When $\lambda$ is normalized with $D$, it increases initially with $P$ until a plateau value of $\sim 0.83$ is reached for the as-cast alloy, which is much larger than that seen in bulk indentation. Relaxation constraint for plastic flow in the bonded interface technique could be a possible reason for this. For the annealed alloy, however, $\lambda/D$ increases continuously, indicating load-dependence of deformation behavior in this material. The inter-band spacing in the as-cast alloy shows a continuous linear increase with the distance from indenter tip, starting at around 1 μm and increasing up to 7 μm over a distance of 40 μm for the 2500 g load. A similar trend is observed in the 5000 g case as well.

Fig. 7 shows the variation of the inter-band spacing for the semi-circular bands, $\varphi$, as a function of radial distance away from the indenter tip, $\xi$, for the as-cast alloy. Close to the indenter tip (for $\xi < 13$ μm) $\varphi$ is constant with an average spacing of $\sim 0.42$ μm whereas it is $\sim 0.72$ μm for $\xi > 15$ μm. The smaller inter-band spacing near to the indent tip points to the presence of a hydrostatic core as averred to in the expanding cavity model. Variation of the angle between the radial bands

as a function of distance from indenter tip was also studied. Away from the tip, it is in the range of 105–118°, with the average of ~110°. Nearer to the tip the band angles are lower lying in the range of 80–90°. This dependence of angle on distance from indenter point, illustrates the pressure sensitivity of the deformation mechanism and are consistent with those predicted by Vaidyanathan et al. [10] for a Zr-based BMG.

To assess the influence of the compliant adhesive interface on the deformation morphology, indentations were performed on interfaces that were held together with the aid of mechanical force in a vice instead of bonding them with the adhesive. No significant differences between the deformation morphologies, with that recorded employing the bonded interface technique, were observed. However, the plastic zone size in the former case is smaller (~36 against 48 μm at a load of 2000 g, for example). Clearly, the compliant adhesive layer does not influence the significant observations made in this study. Though both the techniques employed above do not provide the same amount of constraint that the bulk specimen experiences, they are adequate to get a qualitative insight on the nature of flow of materials under the influence of indentation.

## 4. Discussion

An important observation of this study is that the trends in plastic zone size, both in bulk and interface indentations, are in good agreement with that predicted using the widely accepted expanding cavity model for

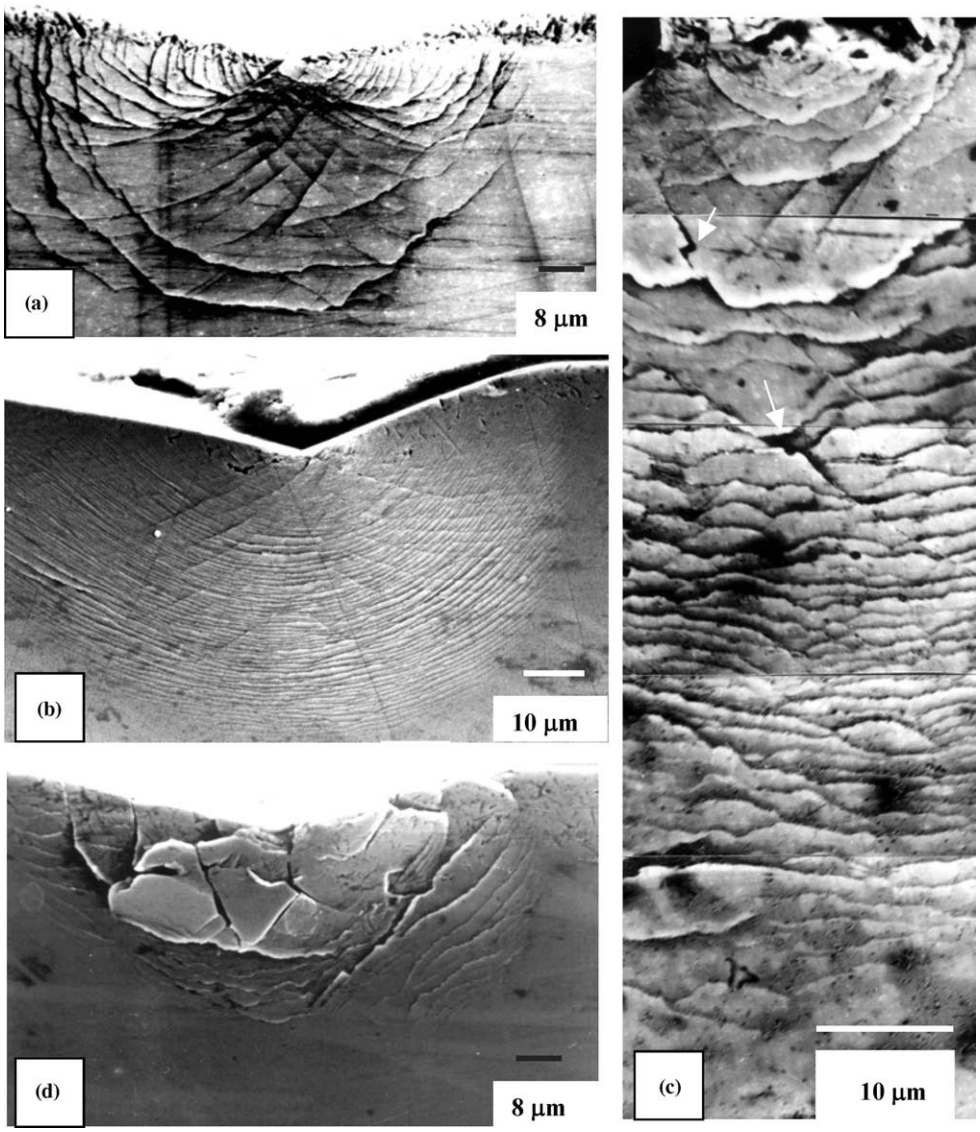


Fig. 5. Morphology of the subsurface deformation zones underneath the Vickers indenter: (a) as-cast alloy subjected to an indentation load of 2500 g. (b) As-cast alloy subjected to an indentation load of 2000 g, exhibiting a semi-circular shear band morphology. (c) Annealed alloy subjected to an indentation load of 5000 g. (d) Fully crystallized alloy subjected to a load of 2500 g, showing extensive cracking.

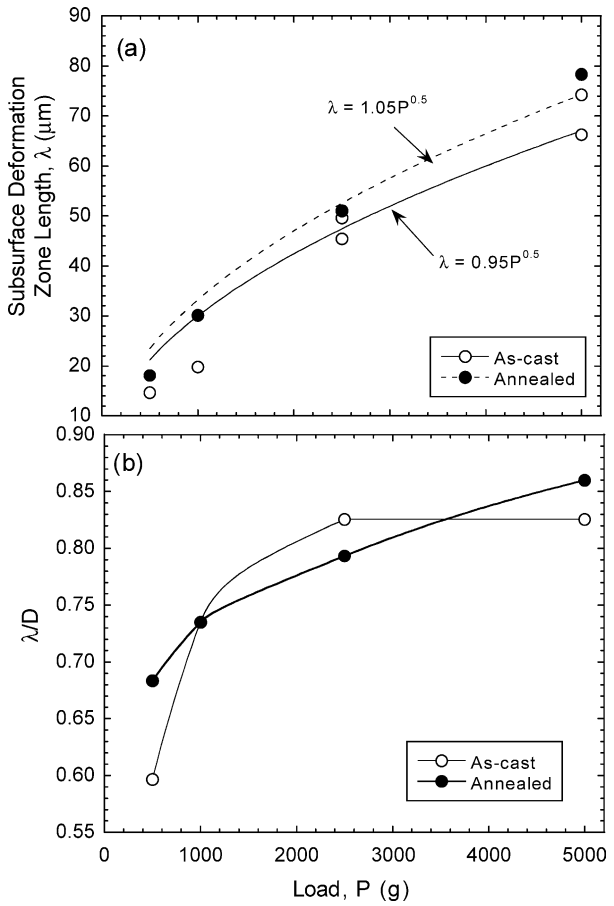


Fig. 6. Variation of (a) the subsurface deformation zone size, $\lambda$, and (b) the ratio of $\lambda$ and the indenter impression diagonal, $D$, plotted as a function of the indentation load for the as-cast and annealed alloys.

the elastic–plastic indentation deformation in crystalline metals. However, the extracted value of $Y$ does not match with that measured in uniaxial compression. One possible reason is that $\delta$ possibly underestimates the actual plastic zone size and hence leads to an abnormally high value for $Y$. Another contributing factor for the observed discrepancy is the pressure sensitivity of deformation in metallic glasses, which leads to a smaller plastic zone vis-à-vis that predicted for a Mises solid, implicitly assumed in the expanding cavity model [10]. The high value of the plastic constraint factor, estimated by comparing $H$ and $Y$, attests this. For solids that exhibit pressure sensitive plastic deformation, Patnaik et al. [18] has shown that for BMGs the $H/Y$ value will be larger than 3.

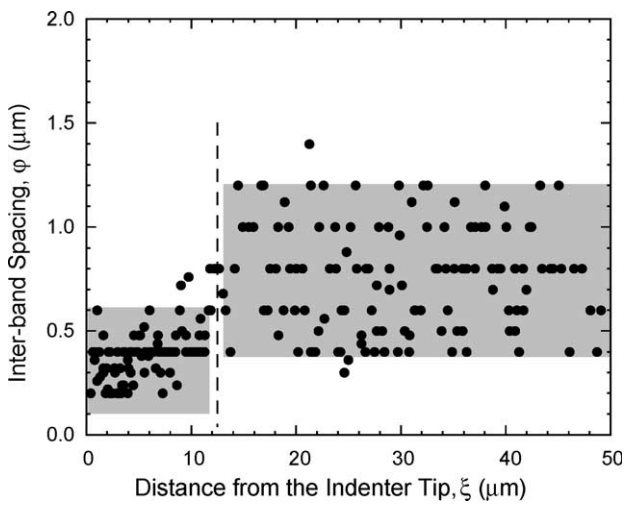


Fig. 7. Variation of the inter-band spacing as a function of distance from the indenter tip, for the annealed alloy at a load of 2000 g.

The deformation morphology in the as-cast alloy is quite different from that seen in the as-cast alloy of a Pd-based glass [21]. While the former closely resembles the plastic flow field of a rigid plastic solid, the latter appears to conform to that of an elastic, perfectly plastic solid for which an expanding cavity model is appropriate. The presence of dendritic crystalline phases in the as-cast microstructure of the Zr-based BMG is possibly a reason for this, necessitating high shear stresses for the onset of shear bands. As a result, the shear band pattern appears similar to the trajectories of maximum shear stress in the slip line field theory of rigid plastic solids [22].

While both the as-cast and annealed Zr-based BMG samples exhibit shear-band dominated deformation zones that are near equal in size, their morphologies are distinctly different, implying a transition in the deformation mechanism. The similarity in $\lambda$ for the partially crystallized alloy and the as-cast alloy implies that the former can accommodate similar amounts of plastic deformation under identical conditions. This is evident from the fact that the incipient cracks observed in the annealed alloy do not propagate unhindered. The tendency for cracking appears to increase with increased crystallization culminating in the observation of severe cracking in the fully crystallized glass. The lack of constraints for crack propagation in toughness tests may be the cause for the precipitous drop in toughness observed in partially crystallized glasses [16].

Finally, a comparison of the results presented in this paper with those obtained during nanoindentation experiments that were carried out on the same group of alloys is warranted. Typically the nanoindentation studies reveal serrated load–displacement ($P - h$) curves [1,4,8], particularly at a lower strain rate; while an increase in strain rate past a threshold value results in non-serrated flow [1]. Schuh and co-workers [1,4] attribute this to the transition from a single shear band to a multiple shear band operation. The macrohardness study reported in the present work is conducted at comparatively high loading rates and also significantly high loads as compared to the nanoindentation tests. The overlapping in-plane shear bands, originating from the indenter tip as seen in Fig. 5a, suggests the simultaneous operation of multiple bands, which has been suggested as a possible reason for the transition from serrated to non-serrated flow. So the deformation morphologies observed corroborates the nature of flow

curves obtained for nanoindentations done at higher strain rate regime.

## 5. Conclusions

Observations of the subsurface deformation zone with the aid of the bonded interface technique indicate to the shear-band dominated deformation zone for both the as-cast and annealed alloys. The density of the radial bands are much more in the glassy state as compared to the semi-circular bands, which dominates when the material is more crystalline, suggesting a transition in the nature of deformation mechanism with annealing. Hardness experiments suggest $H$ is independent of $P$, while for the as-cast alloy $H/Y$ values show pressure sensitivity of yielding criterion. The deformation zone size and the subsurface deformation length increase with the applied load. The BMG studied contained some residual microcrystalline regions, the presence of which may drastically affect the shear band patterns and in general the mass flow processes which determine the band morphology.

## Acknowledgements

The authors wish to thank Profs S. Ranganathan and R. Narasimhan for useful discussions on this work. Funding from the DRDO, Government of India is gratefully acknowledged.

## References

[1] Schuh CA, Nieh TG. Acta Mater 2003;51:87.
[2] Ramamurty U, Kumaran MC. Acta Mater 2004;52:181.
[3] Ramamurty U, Sridhar S, Giannakopulous AE, Suresh S. Acta Mater 1998;47:2417.
[4] Schuh CA, Nieh TG. J Mater Res 2004;19:46.
[5] Kim JJ, Choi Y, Suresh S, Argon AS. Science 2002;295:654.
[6] Lam DCC, Chong ACM. Mater Sci Eng A 2001;318:313.
[7] Pharr GM. Mater Sci Eng A 1998;253:151.
[8] Mukai T, Nieh TG, Kawamura A, Inoue A, Higashi K. Scr Mater 2002;46:43.
[9] Donovan PE. J Mater Sci 1989;24:523.
[10] Vaidyanathan R, Dao M, Ravichandran G, Suresh S. Acta Mater 2001;49:3781.
[11] Wright WJ, Schwarz RB, Nix WD. Mater Trans JIM 2001;42:642.
[12] Fan C, Inoue A. Mater Trans JIM 1999;40:42.
[13] Loffler JF. Intermetallics 2003;11:529.
[14] Basu J, Nagendra N, Li Y, Ramamurty U. Philos Mag 2003;83:1747.
[15] Nagendra N, Ramamurty U, Goh TT, Li Y. Acta Mater 2000;48:2603.
[16] Jana S. MSc (Eng.) Thesis, Indian Institute of Science, Bangalore, India; 2003.
[17] Golovin YI, Ivolgin VI, Khonik VA, Kitagawa K, Tyurin AI. Scr Mater 2001;45:947.
[18] Patnaik MNM, Narasimhan R, Ramamurty U. Acta Mater 2004; in press.
[19] Johnson KL. J Mech Phys Solids 1970;18:115.
[20] Kramer D, Huang H, Kriese M, Robach J, Nelson J, Wright A, Bahr D, Gerberich WW. Acta Mater 1999;47:333.
[21] Jana S, Ramamurty U, Chattopadhyay K, Kawamura Y. Mater Sci Eng A 2004; in press.
[22] Hill R, Lee EH, Tupper SJ. Proc R Soc Lond 1947;A188:273.